Towards the Optimal Antenna-Based Wireless Sensing Strategy: An Ice Sensing Case Study

Mahmoud Wagih, *Member, IEEE* and Junjie Shi

Abstract—Remote ice detection has emerged as an application of Radio Frequency (RF) sensors. While antenna-based "RFID" sensing can detect various measurands, antenna-based sensors are not currently designed based on a systematic methodology, and in most cases may have a low sensitivity requiring specialist hardware or broadband interrogation signals, incompatible with spectrum regulations. Here, we develop a systematic methodology for designing an antenna-based sensor, applicable to measurands inducing a dielectric change in the near-field of the antenna. The proposed methodology is applied to designing printable antennas as highly-sensitive sensors for detecting and measuring the thickness of ice, demonstrating best-in-class sensory response compared to more complex antenna designs. Antenna design is investigated systematically for wireless interrogation in the 2.4 GHz band, where it is found that a loop antenna outperforms a dipole owing to its more distributed capacitance. The antenna's realized gain was identified as the optimum parameter-under-test, with "positive" sensing proposed as a method of improving linearity and immunity to interference. The developed loop antenna sensor exhibits resilience to interference and applicability to different real-world deployment environments, demonstrated through over 80% average ice thickness measurement accuracy and at least 5 dB real-time sensitivity to ice deposition.

Index Terms—Antennas, Antenna Gain, Antenna Sensors, Ice Sensing, Impedance Matching, RF ice sensing, RFID, Materials, Relative Permittivity Measurement, Wireless Sensing

I. INTRODUCTION

R EMOTELY monitoring the accumulation of ice and frost is of great importance to smart cities [1], industrial, and environmental sensing [2] applications. For example, in renewable wind power farms, ice formation on wind turbines can reduce their power output by up to 30% over a year [3]. Recently, several solutions towards ice detection have been realized using Radio Frequency (RF) resonator [4], [5] or antenna-based solutions [4], [6], [7], making it a prime case study for comparing antennas in a dielectric sensing application.

Antenna and resonator-based RF sensing has attracted significant research interest [8], [9], building upon well-established technologies such as RAIN^{TM} RFID [10], and

microwave resonators [11]. Vital signs [12], gases [13], structural health [14], compression [15], temperature [16], humidity [17], and food quality [18] have all been monitored using RF-based sensing for an "RF-enabled" sensory Internet of Things (IoT). In addition, smart sensing materials have been widely studied for their potential use as passive sensors for different parameters [19]. Various topologies and sensing devices from resonant waveguiding structures [11], to radiating antennas have been used for RF sensing [13], [19].

Nevertheless, there is no standardized methodology for designing RF sensors, or a detailed comparison on the effect of different "variables" on the antenna's performance as a sensor. These include the choice of frequency, the sensing element design, i.e. the antenna's geometry, or the RF parameters, such as s-parameters or antenna radiation properties, to be interrogated by the read-out circuit. This results in limited adoption of RF-based sensing in real IoT systems. To illustrate, certain resonant sensors may act as radiators [20], which restricts their real-world deployment due to frequency spectrum regulations requiring re-design [21]. As multiple efforts aimed to present holistic and standardized approaches to wireless sensing, including investigations of the trade-offs between sensitivity and read-range in passive RFID [22], a practical study focusing on the methodology of designing antenna-based sensors is needed. In many antenna applications, such as wireless power transfer [23], wearable communications [24], and additive manufacturing [25], measurement campaigns were carried out to investigate the antennas' performance in their real-world operation environment. However, to the best of our knowledge, such experimental and numerical investigation has not yet been presented for antenna-based sensing applications.

Ice sensing is a prime case-study for RF-based sensors [6], [26]; ice is a low-permittivity and nearly lossless dielectric. While radar-based ice-sounding is a well-defined application of antenna arrays [2], it focuses on thick ice sheets. Recently, microwave two-port resonators were proposed as ice and frost sensors [5], [26], surpassing other visual and optical methods. As resonators require active sampling circuitry, passive RFID tags were investigated for wireless ice detection [6]. We then investigated a 2.4 GHz wire-type antenna as an ice sensor, observing a correlation between the antenna's gain degradation and ice thickness [7]; aperture-type patch antenna sensors were also proposed based on gain measurements at 2.4 GHz [4], and based on S_{11} measurements at 4 GHz [27]. Nevertheless, as with many RF sensing applications, the effects of choosing an RFID tag complex-conjugate antenna [6], a 50 Ω antenna [4], [7], [27], or a two-port resonator [5], [26], on the sensor's performance remains unclear, due to the discussed ambiguity

in RF sensing mechanisms, and the lack of a clear standardized approach to identify the optimal sensing parameter. Furthermore, while both the antenna's gain and impedance were used for sensing in [4] and [27], respectively, it is unclear which RF parameter yields the highest accuracy.

In this paper, we develop and follow a standard methodology for designing an antenna-based sensor for measurands which influence the surrounding dielectric of a sensor, focusing on practical considerations such as frequency spectrum compliance and sensitivity for low-cost read-out circuits. Our key contribution can be divided in two parts:

1) First, proposing and implementing a step-by-step methodology for designing an antenna-based sensor, considering for the first time the impact of frequency allocation and hardware sensitivity.

2) Applying the proposed approach to antenna design for ice sensing, showing that a simple printed loop antenna with a large distributed capacitance, designed as a "positive" sensor whose gain increases in response to the measurand,

Section II introduces the proposed flow for designing RF sensors. In Section III, different antennas are simulated, comparing their performance as ice sensors and evaluating the suitability of different antenna parameters for sensing applications. The fabricated sensors are then characterized experimentally in Section IV, where it is compared to other RF and wireless ice sensing approaches.

II. ANTENNA-BASED SENSING METHODOLOGY

Antenna and resonator-based sensing differs from contactless radar-based sensing in being more resilient to additional interference, and in not requiring an expensive and complex reader circuit with directional antennas. Antenna-based sensors in this work are also distinguishable from "auto-tuning" RFID tags [28], [29], where the changes in the RFID chip's impedance are used to account for and respond to the change in the antenna's impedances.

The sensor's readout is typically observed through the s-parameters [11], [20], for a resonator, or through the far-field gain [6], of a sensing antenna. The real-permittivity (ϵ_r) results in a resonance shift while a change in the $\tan\delta$ of the material results in a change in the antenna or resonator's gain and quality (Q)-factor, respectively.

The most common of RF sensors are two-port resonators, shown in Fig. 1(a), demonstrating high sensitivity for microfluidic and biomedical applications [11], and previously used for detecting freeze events [26]. Such a sensor could be interrogated using a high-sensitivity readout circuit as shown in Fig. 1(a); in a lab environment, this is typically achieved using a Vector Network Analyzer (VNA) or a similar broadband sampling circuit such as a software defined radio [30]. Alternatively, as resonators could be designed with a filter-like response, they could be integrated in chipless RFID tags by connecting them to broadband monopole antennas [31]. Antennas can also be used to directly detect changes in the environment through the gain [4], [6] or the S_{11} response [27]. In this context, RFID antennas can be distinguished
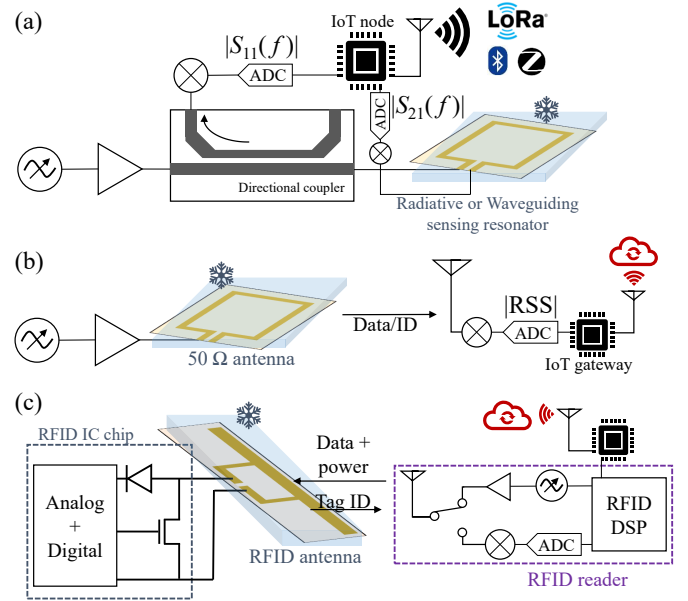

Fig. 1. RF-based sensing approaches and their integration in IoT networks: (a) one/two-port s-parameter sensing [11]; (b) wireless sensing through a 50 Ω-matched antenna gain (this work, [4]); (c) wireless sensing through a battery-less RFID tag's complex-Z antenna gain [6], [14].

from "conventional" antennas, which are designed to match a 50 Ω impedance, applicable to a range of transmission lines and matched active transceivers or amplifier circuitry. RFID antennas however resemble rectennas [32], matched directly to the complex impedance of the UHF RFID IC's RF frontend.

Following the identification of the measurand and its electrical properties (ϵ_r, $\tan\delta$), the sensing topology and subsequently the parameter-under-test (PUT) need to be selected based on the hardware, frequency, and power restrictions, as in as in step 3 proposed RF-based sensing methodology flow, shown in Fig. 2. The first step in designing an RF-based sensor is characterizing the RF effects of the proposed measurand. Along with identifying the measurand's dielectric properties, the potential sources of interference in the operation environment need to be considered and accounted for at the design stage.

To begin with, the frequency spectrum allocation restricts the operation of the sensor. Based on existing regulations, license-free sensors are only allowed to radiate power in the industrial scientific and medical (ISM)-bands, e.g. 868/915 MHz, 2.4 and 5.8 GHz, and the 3-10 GHz UWB spectrum [21]. Moreover, the use of UWB waveforms in the 3–10 GHz spectrum is not covered by the RFID standard [21]. Therefore, unless operating in the UWB spectrum, the interrogation of wireless sensors may be limited to narrow ISM-bands [21]. This prohibits the detection of the resonant frequency f_r, which is impossible to identify without a broadband sweep [6]. Furthermore, two-port resonators based on microstrip technology and operating outside such bands need to ensure full shielding, where microstrip lines are known to radiate with up to −20 dBi gain [33]. Therefore, should s-parameter-based sensing, shown in Fig 1(a), be adopted, the operation has to be restricted to an ISM-band, or utilize a non-radiative RF resonator. Topology (c) builds upon the well-established
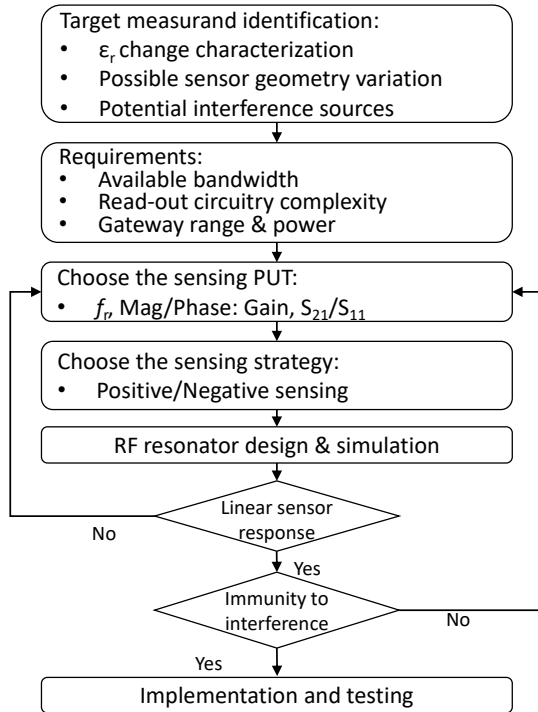
Fig. 2. The proposed RF-based sensor design flow, starting from the measurand definition to antenna optimization for linearity and reliability.
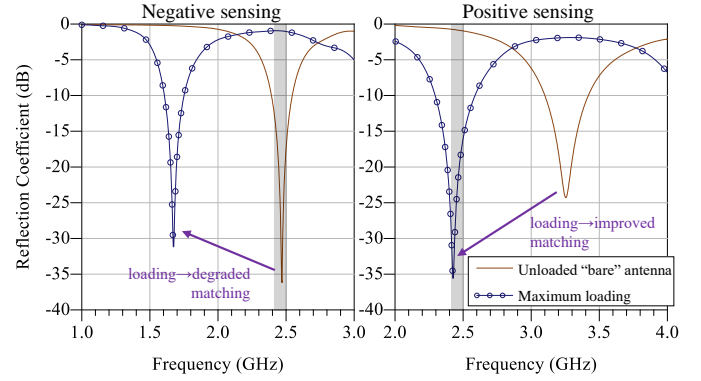

Fig. 3. The principle of positive and negative RF sensing demonstrated through the reflection coefficient (S_{11}) of a resonant antenna sensor; shaded region indicates the read-out frequency.

RFID antenna design principles [34], and is often used as a low-cost battery-free sensor topology [35]. By resizing the sensing element for different frequency bands, the proposed methodology can be adapted for different regulations, regions, and spectrum requirements.

The second restriction relates to the integration with practical hardware such as transmitters and detectors, which affects the PUT. As shown in Fig. 1(a), a coupler is typically needed to measure the reflection coefficient, S_{11}, of a resonator. S_{21} measurement on the other hand are simpler and only require a detector or a down-converter, for measuring the amplitude of the received signal at different frequencies. In most studies, both S_{11} and S_{21} measurements of sensors' response are carried out using a VNA. This enables resolving differences around 0.1 dB [4], which could translate to under 5 mV changes in a typical low-cost RF power detector's output, making it impractical for low-cost IoT implementations based on off-the-shelf parts.

The antenna gain on the other hand could be detected wirelessly, through the received signal strength (RSS) of an active or backscattered transmission [6], which enables a plethora of RFID-based sensing applications [19]. In addition to the topologies shown in Fig. 1(b) and (c), passive circuits such as harmonic transponders [36] can be used to interrogate wireless sensors. Chipless RFID, [31], ultimately has the lowest tag cost, due to not requiring any semiconducting parts, and also represents the least wasteful approach where less electronic components need to be disposed. Nevertheless, it significantly limits the operation range compared to UHF RAIN™RFID. The hardware requirements are also affected by the frequency choice. In a an ISM-band such as the 2.4

GHz band (the frequency of this work), there are additional sources of interference such as Wi-Fi and other IEEE 802.15 sensor nodes. Therefore, a key requirement will be maintaining a sensitivity (i.e. gain change) that is higher than the RSSI uncertainty of the receiver, as well as the RSSI being higher than the noise level coming from interfering signals.

Following the identification of the sensing approach and the wireless regulations, the RF sensing element is designed, as detailed in the next section. The design process involves iterative 3D full-wave electromagnetic simulation to observe the sensor's response to the stimulant for multiple PUTs. At this stage, the performance of positive and negative sensing approaches can be investigated. To explain, a $\Re\{\epsilon_r\}$ will result in a frequency shift in the resonant response of an antenna or a two-port sensor. The antenna could be designed to achieve the maximum gain and minimum S_{11}, under loading, which can improve the read-range of a passive sensor [6], i.e. "positive sensing". Alternatively, the antenna sensor could be designed to achieve the best gain and S_{11} prior to loading, where the stimulus is detected through "detuning", acting as a "negative sensor". Fig. 3 illustrates the operation of a positive and a negative resonant sensor, through the S_{11}. The process of observing the sensor's linear response, evaluating its susceptibility to the anticipated sources of interference, and experimental evaluation is presented in the next sections.

III. ANTENNA SENSOR DESIGN AND SIMULATIONS

The proposed sensor needs to operate in a license-free band, as well as have a response which could be interrogated remotely. Following the methodology in Fig. 2, the key variables which need to be selected to realize the RF-based solution for ice sensing applications are:

1) Parameter-Under-Test (PUT) of an antenna/RF-based sensor. This affects the read-out circuit and can complicate a system beyond typical low-cost IoT hardware.
2) Antenna/resonator design: the active sensing element geometry, materials and its interaction with the loading stimulant. This can maximize and linearize the sensory response in the region of interest.
3) Positive vs. negative sensing: where the PUT either increases or decreases in response to the stimulant.

This can improve the system's immunity to interference, and linearize the sensory response of the antenna's parameters in the range of interest.

To design an antenna-based sensor for wireless ice detection, that is suitable for integration in existing IoT wireless sensor networks, the following sensor criteria need to be met:

1) Maintaining the ability to readout the sensor's response wirelessly, i.e. at the gateway, through the transmitted response from the sensor node, such as using the RSSI.
2) Being compatible with *existing* RF spectrum regulations, confining its readout to ISM bands.
3) Exhibiting a high sensitivity (i.e. in excess of 1 dB) for the sensor to be read using low-cost wireless components such as Universal Software Radio Peripherals (USRPs).
4) At the receiver, the sensor's RSSI must be higher than the neighboring sources of interference (particularly in ISM-bands), to enable the RSSI values to be accurately resolved.

These requirements are first investigated through full-wave simulation, to identify the suitable antenna design for the proposed application. Two antenna sensors are then fabricated and experimentally characterized, under loading, to demonstrate that although all antenna/resonator designs will exhibit some sensitivity to dielectric measurands, only an optimized antenna will act as a linear and interference-resilient sensor.

A. Sensitivity and Linearity Analysis

Comparing the dipole in [6] to the microstrip patches in [27] and [4], a wire-type antenna generally exhibits higher sensitivity to ice. Therefore, "wire-type" antennas are selected as the primary class for the sensor design. Two wire-type antenna designs have been simulated in CST Microwave Studio to evaluate their suitability for ice sensing applications, and identify the ideal PUT, based on the sensing flow proposed in Fig. 2. The antennas are a magnetic loop and an electric dipole, whose dimensions are shown in Fig. 4.

Following on the proposed concept of positive and negative sensing, two variants of each antenna have been designed. The negative-sensing variant is designed to resonate and match 50 Ω at 2.4 GHz, in free space, i.e. before ice-loading. The positive-sensing variant is designed to match 50 Ω at 2.4 GHz under maximum loading, this is when the antenna is completely covered in a thick layer of ice, and is hence smaller than its negative sensing counter-part. The "thick layer" is defined as the thickness beyond which the impedance response of the antenna stops varying, this was determined through the 3D full-wave electromagnetic CST model, by varying the ice superstrate thickness, to be around 50 mm-thick.

As the ice resembles a superstrate which shifts the antenna's frequency response and subsequently alter the gain, an ice layer of varying thickness t (0.1-50 mm) has been simulation on-top of the antennas. As previously reported thickness sensors were demonstrated for t <10 mm ice superstrate thickness measurements, the proposed methodology aims to significantly improve the measurement range through antenna design. The considered dielectric properties of ice are ϵ_r=3.2 and tanδ=0.0009 [37], previously showing a close agreement
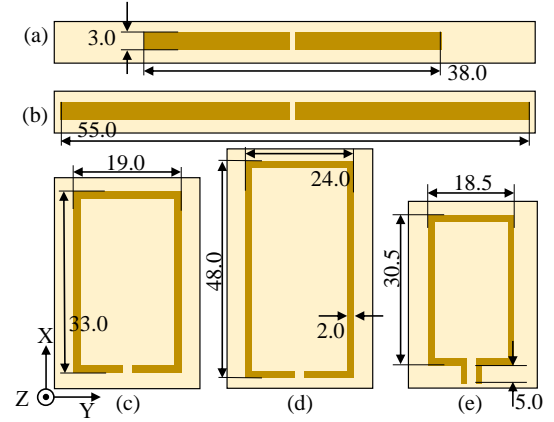

Fig. 4. Layout and dimensions (in mm) of the sensing antennas: (a) positive sensing dipole; (b) negative sensing dipole; (c) positive sensing loop; (d) negative sensing loop; (e) positive sensing loop with extended connector leads.

between antenna simulated and measured impedances [6]. The ice layer is 40×40 cm, substantially larger than the antenna, to mimic the effects of a full ice cover.

Three antenna properties are investigated as the PUT for evaluating their sensitivity to the presence and thickness of the ice layer:

1) ΔG, defined as the change in the antenna's peak gain, normalized to its original unloaded gain, i.e. before the ice layer is deposited onto the sensing antenna. By relying on the *peak* gain, there is strong emphasis on the antenna's radiation pattern's stability under loading.
2) $|S_{11}|$, is the absolute reflection coefficient of the antenna, in the condition considered. While $|S_{11}|$ eliminates the dependence on the wireless interrogation channel, it requires a complex active read-out circuit [38].

For both ΔG and S_{11} only the magnitude is considered as opposed to vector (phase and magnitude) information.

Two of the three PUTs investigated, ΔG and $|S_{11}|$, can be sampled at a single frequency, whereas to identify f_r the S_{11} needs to be sampled over a broad frequency range to find the minimum value. For both ΔG and $|S_{11}|$, the reported values in the next steps are at 2.4 GHz. The antenna's S_{11} response and far-field radiation properties have been simulated for 0 mm< t < 50 mm. Fig. 5 and 6 show the simulated PUTs for positive and negative sensing, respectively, for both the loop and the dipole antennas.

Observing the fitted relations in Fig. 5 and 6, the R^2 exhibits the closest fit for positive sensing, where negative sensing results in R2 <70% for the ΔG and S_{11}, unsuitable for thickness measurements. On the other hand, a broadband sensor which monitors f_r is expected to maintain a high sensitivity and linearity for both positive and negative sensing. Comparing the S_{11} to G, it can be observed that for t >10 mm, the $|S_{11}|$ becomes increasingly non-linear, making it less suited to estimating the thickness of thick ice layers. This is in line with the result presented in [27], where the patch's S_{11} was found to only be suitable for sensing t <7 mm.

Given their highly linear response, the resonant frequency and the antenna gain can be chosen as an ice detection
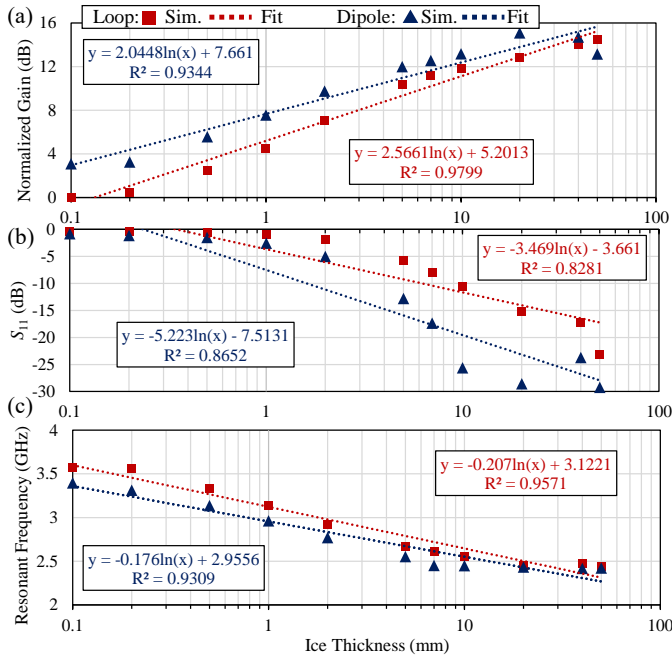
Fig. 5. Simulated antennas' PUTs positive sensing: (a) normalized gain at 2.4 GHz; (b) reflection coefficient at 2.4 GHz; (c) resonant frequency, showing a highly-linear response for the loop antenna for all PUTs.
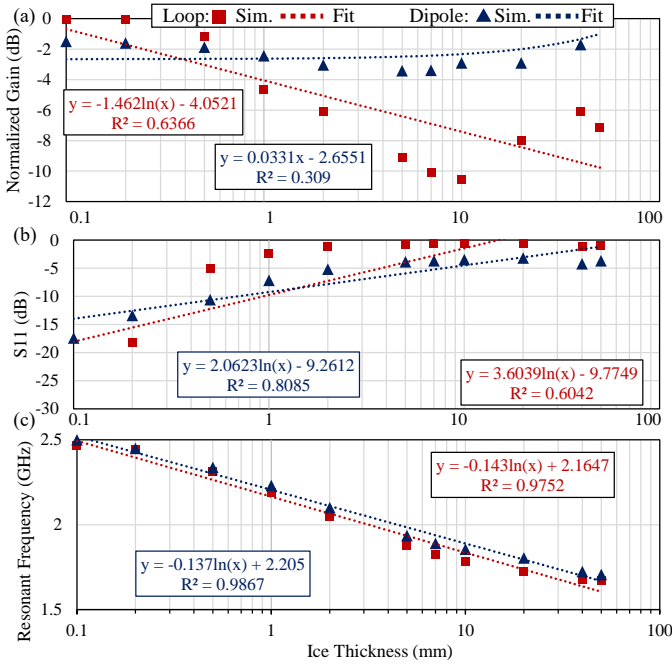

Fig. 6. Simulated antennas' PUTs for negative sensing: (a) normalized gain at 2.4 GHz; (b) reflection coefficient at 2.4 GHz; (c) resonant frequency, showing inferior sensory response in G and S_{11} compared to positive sensing.

PUT. Selecting f_r as the PUT will restrict the real-world implementation to the topology in Fig. 1(a), with a shielded resonator, unless the antenna is scaled to operate in the UWB (3-10 GHz) spectrum. On the other hand, choosing the gain as the PUT enables the sensor to be realized using either of the topologies in Fig. 1(a) and (b). Further observing the gain of both antennas, it can be seen that the dipole antenna

exhibits a higher gain, in Fig. 5(a), which is attributed to its resonant frequency, observed in Fig. 5(c), being closer to the frequency of interrogation (2.4 GHz). This will translate to a small read-range improvement when the dipole antenna is used for $t <10$ mm, before both antennas exhibit a very comparable gain. However, it is important to note that the peak gain is angle-dependent and will rely on the stability of the radiation patterns of the antenna, investigated in Section III-C.

From Fig. 5 and 6, it can be seen that the normalized gain variation, in response to increased ice thickness, is only linear in the positive sensing approach. This is can be explained as follows, in positive sensing, the gain increases due to:

1) improved matching with the source increasing the realized gain, as observed in the S11 response;
2) the ice superstrate acting as a dielectric lens which increases the directivity, later discussed in Fig. 9.

Therefore, it can be seen that the ice influences the antenna's response both through altering its patterns as well as improving the impedance matching, which results in the gain having a higher sensitivity for thicker ice layers. On the other hand, negative sensing relies on detuning to reduce the antenna's gain, whereas the ice layer will still influence the radiation patterns increasing the directivity, which results in an unpredictable gain response for thick ice layers.

The optimization of the sensor through full-wave simulations can also be automated based on an optimization algorithm [39]. The antenna's design goal will be evaluated over a sweep of cases, e.g. ice thickness, for the chosen PUT. For example, the R^2 of the gain-thickness relation could be used as the optimization goal, to maximize the linearity of the sensor.

B. Equivalent Circuit Analysis

To further understand the capacitive sensing mechanism of both antennas, a simple equivalent circuit model has been extracted. As both antennas are primarily composed of coplanar strips, the per-unit length coplanar stripline capacitance and coplanar inductance models were used to calculate the capacitance and inductance of each antenna [40]. Fig. 7(a) and (b) show the calculated reactive equivalent circuit model, which can be used to calculate the resonant frequency of the sensing antennas.

To simplify the analysis, the antenna's are assumed to operate in space, due to the very low thickness of the substrate. The ice loading is assumed to behave as a uniform coating over the top plane of the antenna, as denoted by C_{sense} in Fig. 7(c). To simplify the calculation, the analytical circuit model is only used to calculate the resonant frequency. To explain, the antenna's radiation resistance is expected to vary over frequency. In the simplified equivalent circuit model, it is assumed that the resistive element is solely formed of a radiation resistance element equal to 50 Ω. Fig. 7(e) shows the full-wave simulated and closed-form calculated S_{11} of the loop antenna.

Despite the simplification of the model to exclude the substrate's permittivity and the frequency-dependence in the resistance, the analytical LC model follows the full-wave
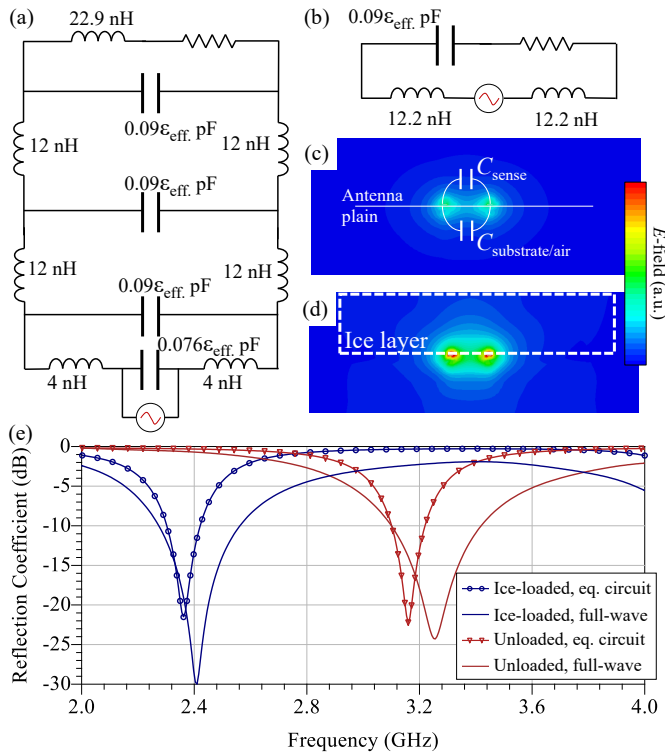
Fig. 7. The capacitive sensing approach of the loop and dipole antennas: (a) loop antenna equivalent circuit; (b) dipole antenna equivalent circuit; (c) simulated unloaded E-field of the loop at 2.4 GHz; (d) simulated loaded (40 mm-thick ice) E-field of the loop at 2.4 GHz; (e) simulated and calculated S_{11} using the equivalent circuit model in (a).

Fig. 8. Simulated gain-thickness response of the positive-sensing loop for varying humidity levels and water levels.

behaviour. To emulate the ice loading in the equivalent circuit, an effective loading permittivity term $\epsilon_{\text{eff.}}$ is introduced to vary the capacitance. $\epsilon_{\text{eff.}} = 1.6$ is chosen as ($\epsilon_{\text{ice}}/2$) to reflect that the ice only loads half of the antenna's capacitance, as observed in the unloaded and loaded E-field plots in Fig. 7(c) and (d), respectively. From the closed-form loaded S_{11}, in Fig. 7(e), it can be seen that the simplified capacitive sensing model closely approaches the full-wave response.

In light of the closed-form model, and observing the lumped elements model of both antennas, it can be seen that the loop antenna has a higher and more distributed capacitance. Therefore, in the proposed positive sensing application, it can be seen that a larger antenna with a higher overall sensing capacitance will result in an improved sensory response.

C. Interference Susceptibility and Reliability

The final step prior to prototyping, as shown in Fig. 2, is investigated the sensor's immunity to false-reads or misses. This could be due to external environmental factors, such as being loaded with water or changing ambient conditions.

The relative permittivity of the Kapton substrate is dependent on the humidity level, which could shift the resonance of the proposed RF ice sensing antenna [41]. Polyimide's ϵ_r increases linearly with humidity, where ϵ_r equals 3.1, 3.5, and 3.8, for 10%, 50%, and 100% humidity levels, respectively [42]. The aforementioned values were used to simulate the antenna's PUT, the gain, for varying ice thicknesses. In Fig. 8,
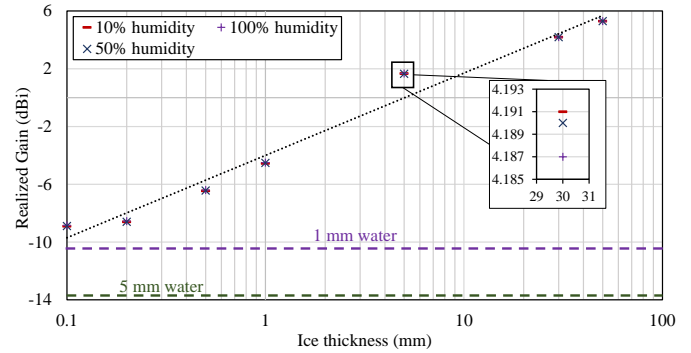
it can be observed that the gain change due to humidity is insignificant compared to the ice superstrate, which validates the sensor's immunity to humidity-induced interference. As for temperature effects, the change in the permittivity of Kapton is significantly lower than that caused by humidity [42]. Therefore, the printed antenna's response will not change for different temperatures.

The other source of interference expected in an ice sensor is water droplet accumulation on the surface of the sensor. Water is characterized by a very high ϵ_r compared to ice [37], therefore, a thin layer of water, depositing directly over the sensor, may result in a similar frequency shift to that caused by a thick ice layer, causing a false match. Fig. 8 shows the simulated antenna's gain for 1 and 5 mm of water, where it can be observed that for both cases the antenna's gain is lower than that under all conditions of ice loading. This is attributed to the high conductivity of water which results in a low antenna efficiency due to absorption by the water molecules.

The observed response to water highlights the benefits of the proposed positive sensing methodology, as well as the chosen PUT. To explain, the presence of water on the sensor results in a matched $S_{11} < -10$ dB, which shows that should the S_{11} be selected as the PUT, the sensor will not be able to distinguish frost events from water droplets caused by rain or dew. Furthermore, should a negative sensing approach be adopted, i.e. where the gain reduces in response to the ice, then the presence of water will also result in a false-match, where the presence of water will always be interpreted as a thick layer of ice, due to water's high $\tan\delta$. Therefore, according to the decision-making strategy introduced in Fig. 2, selecting the realized gain as the PUT is more suitable for remote sensing of the presence of ice than the resonant frequency.

Selecting the gain as the PUT and positive sensing as the design strategy, the final parameter which control the robustness of such a wireless antenna sensor is the radiation pattern. To explain, the angular direction of the peak gain needs to be stable for the gain change to be detected wirelessly. Otherwise, if the direction of the antenna's main lobe changes, wireless detection will not be possible and the change in the gain will not be read successfully by the receiver, resulting in angular "blind spots" in the antenna's scanning beamwidth. Fig. 9 shows the simulated 2.45 GHz realized gain pattern of
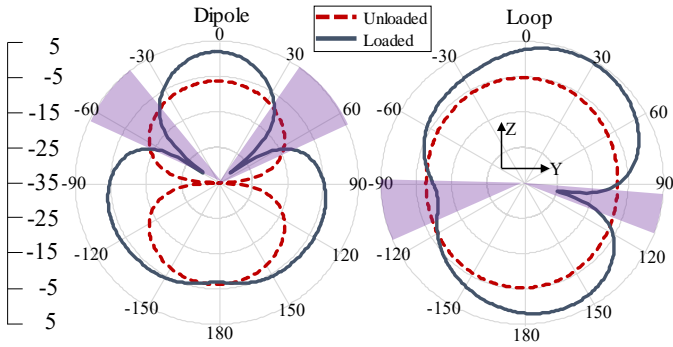
Fig. 9. Loaded (solid) and unloaded (dashed) realized gain patterns (dBi) of the positive sensing dipole (left) and the loop (right) sensors; the shaded regions indicate the angles at which the loaded gain is lower than the unloaded gain.
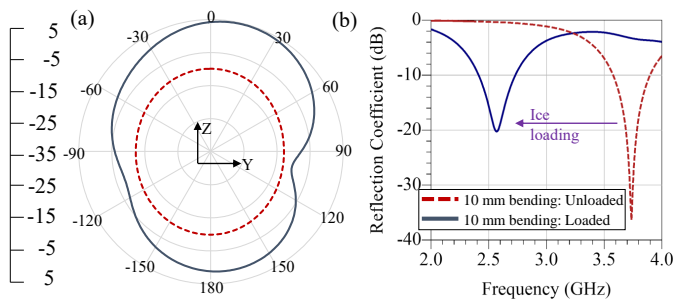

Fig. 10. The effect of bending over a 10 mm radius on th loop antenna: (a) realized gain patterns; (b) reflection coefficient.
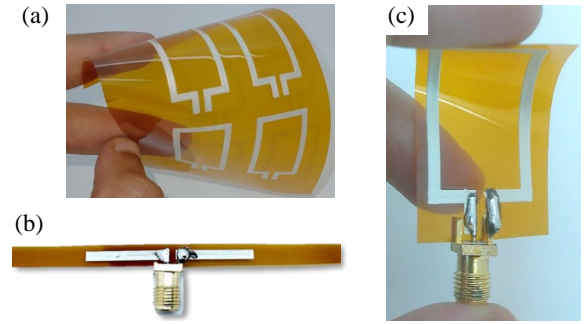

Fig. 11. Photographs of the fabricated antenna sensors: (a) printed traces on polyimide; (b) connectorized dipole antenna; (c) connectorized loop antenna.

bending is presented in Section IV-B (Fig. 16).

IV. SENSOR FABRICATION AND MEASUREMENTS

A. Additively-Manufactured Sensors Characterization

The designed antennas have been fabricated on a flexible polyimide substrate of 75 μm thickness. Direct-write dispenser printing, recently demonstrated for energy harvesting [25] and IoT antenna prototyping [43], has been utilized to deposit the silver tracks on the organic polymer substrate. The printer used is a commercially-available Voltera V-one printer, intended for rapid and low-cost PCB prototyping. The designed antenna traces are directly printed on the polyimide substrate, adhered to a planar surface, without the need for a screen or a photolithography mask. The printed silver traces are cured at 170° for 50 minutes, using a standard hotplate. Once cured, SMA connectors are mounted using low-temperature solder and encapsulated using Kapton tape which enables a reliable connection to other coaxial components such as test cables Fig. 11(b) and (c) show the connectorized dipole and loop antenna, respectively.

As a relatively low conductivity (σ=1.05×10^{6}S/m) silver ink is used, different conductors such as conductive textiles or conductive polymers can be used to realize the antenna. While lower conductivity inks or materials will result in a lower antenna gain and consequently a lower read-range, they will not influence the antenna's sensory response, as the ice primarily influences the capacitance and the radiation pattern, whereas the resistivity of the antenna will influence its efficiency.

The fabricated antennas have been characterized using a Rhode & Schwarz ZVB4 VNA calibrated using a standard TOSM calibration kit. The VNA was used to measure the antennas' unloaded reflection coefficient (S_{11}) response, and upon-loading, the S_{21}, as detailed in the next section. Fig. 12 shows the simulated and measured S_{11} of the fabricated positive and negative sensing loops from Fig. 4(d) and (e). The observed good agreement between simulation and measurement validates the models and indicates that the antennas' sensory response will be in-line with the numerical values.

B. Ice Detection and Monitoring

The first application of the proposed sensor is to detect the formation of ice in real-time. To evaluate the sensor's

the positive sensing loop and dipole, before and after 40 mm-thick ice loading, where the blind spots are shaded. The loop antenna exhibits a gain of and 4.4 and -5.3 dBi when loaded and unloaded, respectively, whereas the dipole exhibits a a gain of 5.47 and -6.3 dBi for the loaded and unloaded cases, respectively. It is essential to note that the quoted values include the additional printed ABS substrate and are for the loop antenna in Fig. 4(e).

Observing the main-lobe direction for both antennas, it can be seen that the loop's main-lobe direction is maintained at $-90° < \theta < 90°$, indicating that the sensor's output will be consistent across the broadside hemisphere. The dipole's main beam, however, changes its angular response. Therefore, should the dipole-based sensor be interrogated around $\pm30° < \theta < \pm60°$ (the shaded region), the presence of ice will not be detected due to the change in the radiation pattern. Therefore, it is expected that the loop antenna will exhibit a clearer sensor response. This will be validated in the next section, by observing the sensor's response at $\theta \approx 30°$.

As the antenna will be printed on a flexible substrate to conform to different surfaces, the effect of bending needs to be characterized. Fig. 10 shows the simulated realized gain patterns and S_{11} of the loop antenna when bent over a 10 mm radius. For both cases, the 40 mm-thick ice loading induces a very similar response in the radiation pattern to the flat antenna, in Fig. 9, despite the resonance shift to a higher frequency for both the loaded and unloaded cases. A real-world experimental demonstration of the antenna sensor under
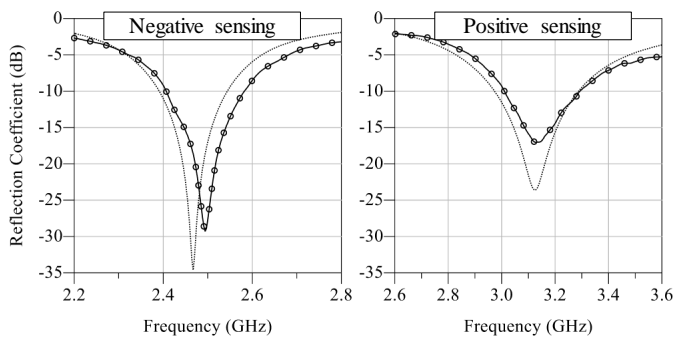
Fig. 12. Simulated (dashed) and measured (solid) reflection coefficient of the loop positive sensing, from Fig. 4(e), and negative sensing, Fig. 4(d), antennas.

Fig. 14. Measured time-variant RSS (S_{21}) received from the loop antenna at 2.47 GHz under different loading events; dashed grey line indicates the unloaded bare antenna RSS.
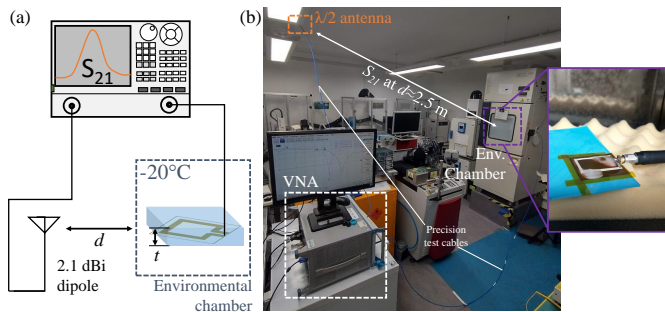

Fig. 13. Measurement setup of the proposed ice sensor: (a) schematic; (b) photograph of the setup utilizing an environmental chamber, with the reader antenna positioned approximately 30° off the ice sensing antenna's broadside direction.

performance, the antenna has been connected to a VNA's port with a standard $\lambda/2$ dipole on the second port, as shown in Fig. 13(a). The printed sensing antenna was placed inside a WKL100 environmental chamber, which enables setting the ambient temperature down to −50°C, while measuring the antenna's S_{11} and S_{21} response using a precision test cable, as shown in Fig. 13(b). The measured S_{21} will be indicative of the RSS received from an ice-sensing node.

The loop antenna, expected to achieve high sensitivity based on simulations, was placed in the environmental chamber at −20°C with a printed ABS support layer. The "reader" antenna, a standard wire dipole, was placed at $d \approx 2.5$ m from the sensing antenna (inside the climate chamber) at an angle around 30°. Recalling Fig. 9, the loop antenna's gain is expected to be stable in this direction, whereas the loop antenna sees a null when loaded with ice. In a real-world application, the distance is limited by the sensitivity of the receiver, which often allows up to 100 m separation between a typical Bluetooth or Zigbee node and the gateway. The RSS was measured before any loading to be around −56 dB, as shown at time=0 in Fig. 14. Water droplets are then added onto the loop antenna, causing a deterioration in the RSS due to water's high tanδ. Following the addition of water, the RSS decays further, which is attributed to the increase in the water's tanδ as its temperature approached 0°C prior to freezing. Due to the small volume of water, freezing occurs in 1 minute, which results in an increase in the RSS, beyond the unloaded sensor's response, as shown in minutes 1-2 in Fig. 14. This
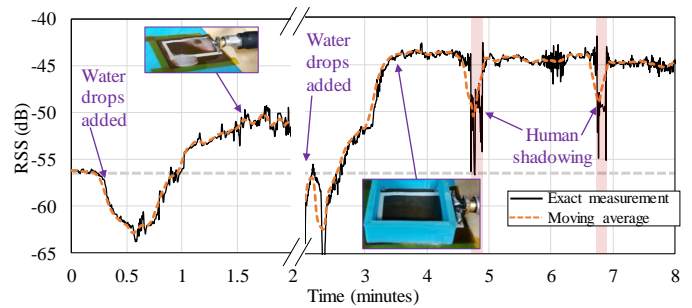
validates the proposed positive sensing mechanism, where the gain of the antenna has increased by over 4 dB, in response to the small ice formations observed in the inset photograph at minute 2 in Fig. 14.

Further water droplets have been added to the sensor to observe the detection of thicker ice layers. The RSS drop at 2–3 minutes is attributed to the losses in the water droplets, where the RSS drops further after the water cools down, for about 0.2 minutes, prior to freezing. As soon as the additional water droplets froze, the RSS improves by a further 7 dB compared to the first loaded gain. This indicates that the proposed antenna is not only sensitive to ice forming on its surface but can also be used to measure its thickness.

The same process was repeated for the dipole antenna, from Fig 11(b), fabricated as a practical reference, to observe its response to freeze events. The dipole is expected to exhibit an inferior sensory response to the loop in terms of the gain change and radiation patterns instability. Nevertheless, its response may still indicate the presence of ice. As observed in Fig. 15, the addition and freezing of water droplets can be detected in real-time, with a similar trend to that of the loop antenna sensor. Nevertheless, by comparing the loaded RSS, at 4 minutes, to the initial RSS, it is observed that the change in the gain is around 1 dB, which is more difficult to detect compared to the loop antenna which exhibited at least 4 dB sensitivity, which improves to >10 dB under thick ice-loading. This is explained by the change in the radiation patterns of the dipole, previously observed in Fig. 9, where the interrogation angle≈40∘ in the broadside direction results in the measurements taking place in the dipole's blind spot. Therefore, antennas with unstable radiation patterns cannot be used to determine absolute gain values. Nevertheless, should the dipole be applied to a real-time sensing system which monitors a water flow, freeze events can be detected through the change in the total efficiency, which results in the gain improvement between 1.2 and 3 minutes in Fig. 15.

From the time-variant RSS measurements, it can be observed that the uncertainty arises from external factors which would degrade the RSS. For example, in Fig. 11, the line-of-sight (LoS) human body shadowing between the transmitting and the receiving antenna would reduce the instantaneous RSS to a level below the ice detection threshold. However, such LoS blockage is likely to be temporal, and will not influence
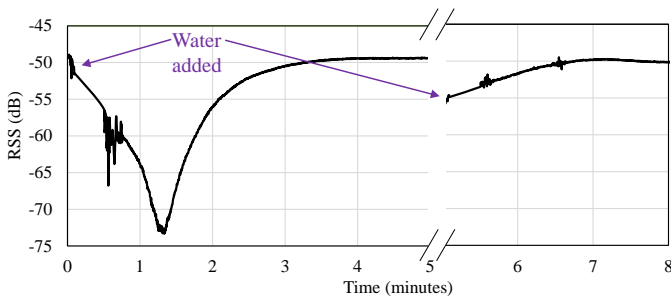
Fig. 15. Measured time-variant RSS from the dipole antenna at 2.47 GHz (the reference sensor design) for two consecutive freeze events.
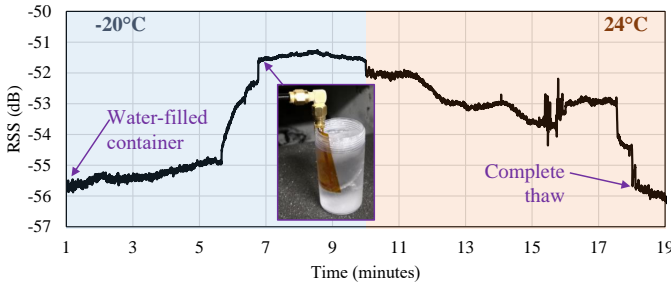

Fig. 16. Measured time-variant RSS (S_{21}) from the submerged loop antenna emulating an in-pipe IoT monitoring system application.

Fig. 17. Measured S_{11} and S_{21} of the unloaded and ice-loaded antenna with and without the close proximity of a terminated ("receiving") antenna; inset shows measurement configuration.

the performance of the system over a long sampling period, and can be filtered out using a moving average filter. As shown in Fig. 14, the moving average, with a 1 s window and a 5 Hz sampling, trace is not susceptible to the introduced interference, and will enable a correct detection of the ice.

The presence of water droplets around the antenna, in presence of the ice, can also mask the sensor's response. This is observed in Fig. 14 at 2–3 minutes, where the measured channel gain degrades when water droplets were added to an iced antenna, due to the absorption in the water droplets. However, interference from water will also be temporal, where the ambient freezing temperature in a deployment environment will result in the additional water droplets (from precipitation or dew) freezing, as observed in Fig. 14, from minutes 3–3.5.

A key application of ice and frost detection is frozen water pipes [44]. As the proposed antenna is implemented on a flexible substrate, it can conform to fit inside water pipes. A plastic tube was used as a water container where the antenna is attached and placed inside the environmental chamber, set to $-20°$C. The tube was filled with water submerging the embedded antenna. The measured time-variant S_{21} of the freezing water pipe is shown in Fig. 16, with the inset showing a photograph of the tube following a complete freeze. The observed RSS change of over 4 dB to the water freezing demonstrates that the proposed sensor could instantly detect the presence of ice. Given that the S_{21} measurement was performed inside the environmental chamber's enclosure, which combines several metallic and insulating surfaces, it can be concluded that freeze events could be detected using deeply embedded antennas in inaccessible locations.

As the antenna relies on the interaction with the ice layer in the near-field, its sensory response might depend on close
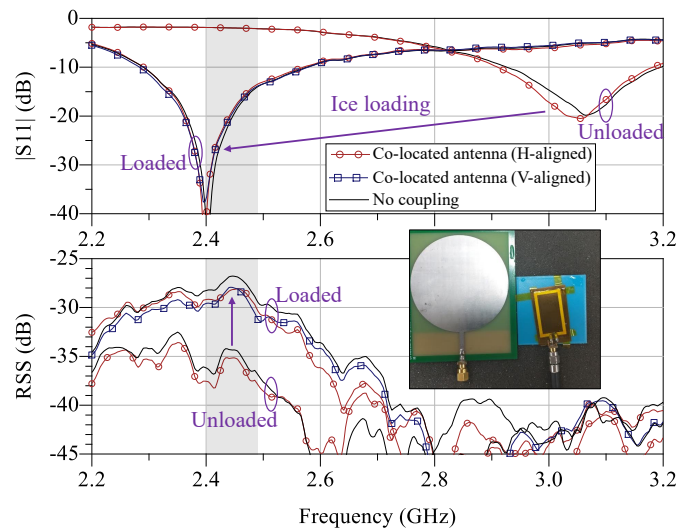
coupling with other antennas. To investigate the effects of close proximity to other antennas, the sensing loop antenna was positioned at less than 2 cm ($< \lambda/4$) from a terminated broadband antenna, which emulates an active receiver, as shown in the inset of Fig. 17. The antenna's S_{11} as well as the channel gain between the sensor and a 70 cm-separated "reader" patch antenna were measured before and after ice loading, as shown in Fig. 17. The co-located antenna was aligned horizontally (H) and vertically (V), to observe the influence of alignment on the sensor's readings.

In both the loaded and unloaded far-field RSS responses, it can be seen that the gain decreases by approximately 1 dB, when the terminated "receiving" antenna is in close proximity. This is attributed to the antenna absorbing part of the sensor's radiated fields, which results in an overall lower channel gain. However, as the proposed sensor exhibits a high sensitivity that exceeds 5 dB, both the loaded and unloaded RSS are very distinguishable, as in Fig. 17, showing the sensor's resilience to being deployed in very close proximity to other antennas. Should the co-located antenna act as a transmitter, it is expected that the sensor's response will be maintained and will still be detectable by the reader, as the sensor will have its own unique ID. The observed sensory response, both in the presence and absence of the co-located antenna, falls within the RSSI accuracy of smartphones [45], which shows that the proposed sensor could be adopted in future wireless networks.

C. Remote Ice Thickness Measurements

The linear relation between the thickness and the antenna's gain, in Fig. 5, shows that the proposed antenna can be used to remotely measure the thickness of the ice. A similar setup to Fig. 13(a) was used to measure the ice thickness t, with the exception of the measurements taking place outside the environmental chamber, to avoid variations in the antenna's radiation patterns due to the metal enclosure. 3D printed molds were used to contain the ice used in the thickness investigation.

Fig. 18 shows the broadband measured S_{21}/RSS between the loop and the "reader" dipole, along with the loop's S_{11}.

The simulated ice thickness-gain relation, from Fig 5(a), was used to calculate the thickness of the ice, based on the measured variation in the antenna's gain. The thickness of the ice was evaluated using

$$t = z \times \exp\left(\frac{\Delta G - x}{y}\right), \tag{1}$$

where x and y are the curve fitting exponents obtained from the CST simulated thickness-gain relation, as x=5.20 and y=2.57, based on the fitted simulated response from Fig. 5(a), ΔG is the measured change in the RSS, caused by the antenna's gain improvement, and z is an empirical tuning parameter, to account for the measurement tolerances due to air gaps between the antenna and the placed ice samples. The tuning parameter z is deduced by performing an initial RSS measurement with the sensor under maximum loading, to calibrate the standard deviation out of the measurements, and is found to be z=1.39. Instead of using actual ice for the determination of z, which may be practically impossible at the deployment time, a 3D printed dielectric phantom [46] with a comparable ϵ_r to that of ice, or more broadly the measurand investigated, could be used for post-fabrication tuning.

Fig. 19 shows the RF-measured ice thickness compared to the ground truth thickness, where the maximum error percentage is under 20%. Averaging the measurement error across the different ice thicknesses investigated, the sensor achieves a 91% accuracy in remotely quantifying the thickness of the ice layer over the antenna, using wireless far-field gain measurements. Therefore, the proposed sensor could be reliably used to not only detect frost events, but also to quantify the accumulating ice, enabling its use, for example, in monitoring wind turbines [47], with the sensor and the gateway located at a fixed distance (e.g. at the turbine's rotor).

While the S_{11}, in Fig 18, exhibits a similar measured response to thicker ice layers, when t was evaluated based on the S_{11} the average error was found to be around 40%. This further validates the results in Section III, where the far-field G was found to be the most linear PUT. Furthermore, the linear and accurate response of G as the PUT validates the proposed methodology of systematically investigating the different PUTs to reach the optimal sensing performance, unlike previous sensors where the PUT choice was not justified with respect to the sensitivity [4], [6], [27].

D. RF Ice Sensing in Future Wireless Sensor Networks

The proposed sensor could be applied in a variety of industrial and smart cities wireless sensor network usecases, a single IoT-connected gateway could act as a sink for the sensor output from several data acquisition nodes, based on the proposed antenna. The conformable sensing antennas could be deeply-embedded within water or gas pipes, or retrofitted as "smart-skin" on important assets or surfaces [48]. Further performance gains in terms of power and size reduction could be achieved based on state-of-the-art solid-state transceiver circuits. To explain, low-power single-chip 2.4 GHz transceivers have been proposed [49], which could integrate with the printed antenna
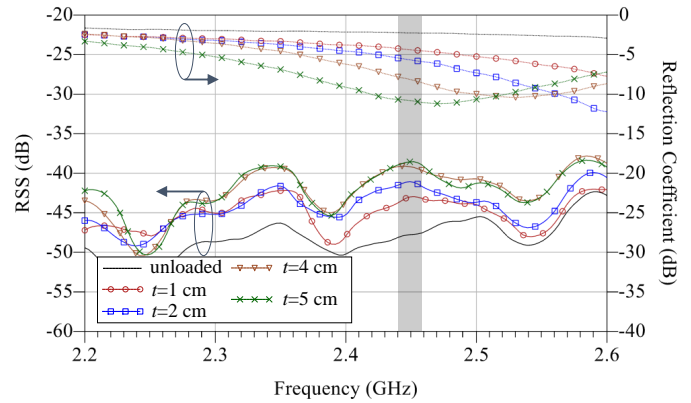

Fig. 18. Measured RSS (solid lines) between the sensing loop and the standard dipole, along with the reflection coefficient (dotted lines) of the sensing antenna for varying ice thicknesses.
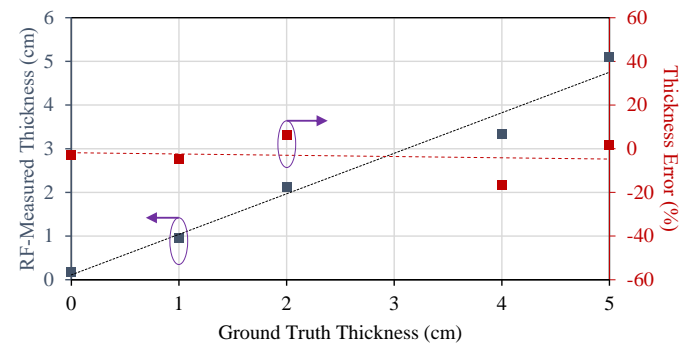

Fig. 19. Remotely measured ice thickness based on the gain and the relative measurement error for 0 mm$< t <$ 50 mm.

for pervasive deployment. By measuring the sensor nodes' unloaded RSS and then monitoring the time-varying RSS, the build-up of ice could be rapidly detected even during temporal LoS shadowing, as seen in Fig. 14. The developed sensor based on the proposed sensing methodology could also be integrated in a variety of IoT node architectures. For example, should the antenna be connected to a 50 Ω-matched RF energy harvesting rectifier [32], a passive RFID system, as in 1(c), could also utilize the proposed antenna for ice detection.

Table I compares the developed loop antenna to recently reported RF-based ice sensors, where it can be observed that the proposed sensor achieves the highest accuracy and thickness measurement range. Moreover, the proposed solution is the most scalable to different frequency bands, antenna designs, and read-out circuits. For example, the resonators in [5], [26] can only be interrogated using the active circuitry shown in Fig. 1(a), increasing the complexity beyond that of a typical IoT node. Furthermore, while antenna-based far-field sensing at 2.4 GHz was previously proposed in [4], the patch antenna's gain change is under 1 dB, implying that multi-tone measurement is required across the 2.4-2.5 GHz spectrum to identify the resonant peak, in addition to requiring more sensitive detector/ADC circuitry to resolve the <1 dB gain change. Therefore, the higher sensitivity achieved by the proposed sensor antenna enables simpler and lower resolution readout circuitry, where a minimum RSS variation of 5 dB,

TABLE I
COMPARISON WITH RECENT RF ICE SENSORS

	This work	2021 [6]	2021 [4]	2021 [27]	2019 [26]
Sensor type	**Loop antenna**	RFID tag	Patch Antenna	Patch Antenna	μstrip Res-onator
Freq. (GHz)	**2.4**	0.868	2.4	3.9	3.5-5.0
PUT	G	G	G	S_{11}	S_{21}
Wireless read	**Yes**	Yes	Yes	No	No
t meas. range	**0-50 mm**	NA*	0-25 mm†	8 mm	NA*
t accuracy	**>85%**	NA*	NA	$\approx$70%‡	NA*
Elec. size (λ^2)	**0.28× 0.15**	0.32× 0.01	0.48× 0.54	$\approx$0.4× 0.4	0.56× 0.70
Sensitivity	**5–15 dB**	$\approx$5– 20 dB	$\approx$2– 5 dB	$\approx$1– 7 dB	NA

*No t measurement, detection-only sensor; †Simulated thickness, no experimental thickness measurement; ‡ evaluated from the graph; NA: not applicable.

and up to 15 dB, was seen in Fig. 14, as the ice thickness was increased. Furthermore, the accuracy of determining the thickness is over 85%, with a maximum error of -15% (at t=4 cm, as seen in Fig. 19. Finally, while battery-free ice sensing RFID tags were proposed in [6], the approach is limited to complex-conjugate RFID antennas and is not transferable to different frequency bands or communication protocols. In addition, the read range of such RF-powered RFID sensors will be restricted by the RFID tag sensitivity, which can only be interrogated up to 10 m [50].

V. CONCLUSION

In this paper, a standard methodology was proposed and investigated for designing RF sensors, towards enabling low-cost and pervasive RF-enabled sensor networks. Remote ice detection and monitoring was investigated presenting a loop antenna sensor operating at 2.4 GHz, with a state-of-the-art sensory response. The key aspects of designing an antenna-based s can be summarized as

1) The sensors' PUT is the most influential variable which controls the accuracy, where >85% accuracy was achieved by interrogating the gain instead of the S_{11};
2) Positive sensing, where the antenna's gain improves in response to loading, in this case ice build-up, presents the highest linearity and immunity to interference;
3) The stability of the radiation patterns of a sensing antenna is paramount, and could render certain antenna designs, e.g. the printed dipole in this study, unsuitable for their wireless sensing application.

Compared to recently reported sensors, the proposed flexible and printed antenna is highly suitable for rapid and accurate wireless detection of ice in future smart cities. It is anticipated that the proposed methodology will underpin various RF-enabled sensing applications, simplifying the design and implementation of RF-enabled IoT wireless sensors.

REFERENCES

[1] I. Zhou, J. Lipman *et al.*, "Frost monitoring cyber–physical system: A survey on prediction and active protection methods," *IEEE Internet of Things Journal*, vol. 7, no. 7, pp. 6514–6527, 2020.

[2] J.-B. Yan, R. D. Hale *et al.*, "A Polarization Reconfigurable Low-Profile Ultrawideband VHF/UHF Airborne Array for Fine-Resolution Sounding of Polar Ice Sheets," *IEEE Transactions on Antennas and Propagation*, vol. 63, no. 10, pp. 4334–4341, 2015.

[3] K. Wei, Y. Yang *et al.*, "A review on ice detection technology and ice elimination technology for wind turbine," *Wind Energy*, vol. 23, no. 3, pp. 433–457, 2020.

[4] R. Kozak, K. Khorshand *et al.*, "Patch antenna sensor for wireless ice and frost detection," *Sci. Rep.*, vol. 11, p. 13707, 2021.

[5] R. Kozak, B. D. Wiltshire *et al.*, "Modified microwave sensor with a patterned ground heater for detection and prevention of ice accumulation," *ACS Applied Materials and Interfaces*, vol. 12(49), pp. 55 483–55 492, 2020.

[6] M. Wagih and J. Shi, "Wireless Ice Detection and Monitoring using Flexible UHF RFID Tags," *IEEE Sensors Journal*, pp. 1–1, 2021.

[7] J. Shi and M. Wagih, "Flexible Direct-Write Printed RF Sensor for RF Ice Sensing," in *2021 IEEE International Conference on Flexible and Printable Sensors and Systems (FLEPS)*, 2021.

[8] P. Mezzanotte, V. Palazzi *et al.*, "Innovative RFID Sensors for Internet of Things Applications," *IEEE Journal of Microwaves*, vol. 1, no. 1, pp. 55–65, 2021.

[9] G. Marrocco, L. Mattioni, and C. Calabrese, "Multiport Sensor RFIDs for Wireless Passive Sensing of Objects—Basic Theory and Early Results," *IEEE Transactions on Antennas and Propagation*, vol. 56, no. 8, pp. 2691–2702, 2008.

[10] B. S. Cook, J. R. Cooper, and M. M. Tentzeris, "An Inkjet-Printed Microfluidic RFID-Enabled Platform for Wireless Lab-on-Chip Applications," *IEEE Trans. Microw. Theory Techniq.*, vol. 61, no. 12, pp. 4714–4723, 2013.

[11] A. A. Abduljabar, D. J. Rowe *et al.*, "Novel microwave microfluidic sensor using a microstrip split-ring resonator," *IEEE Transactions on Microwave Theory and Techniques*, vol. 62, no. 3, pp. 679–688, 2014.

[12] X. Hui, J. Zhou, and E. C. Kan, "High-Volume Parallel Mouse Vital-Sign Monitoring With Near-Field Coherent Sensing," *IEEE Antennas and Wireless Propagation Letters*, vol. 19, no. 7, pp. 1152–1156, 2020.

[13] L. Yang, R. Zhang *et al.*, "A Novel Conformal RFID-Enabled Module Utilizing Inkjet-Printed Antennas and Carbon Nanotubes for Gas-Detection Applications," *IEEE Antennas Wireless Propag. Lett.*, vol. 8, pp. 653 – 656, 2009.

[14] Y. He, M. M. Li *et al.*, "A Passive and Wireless Sensor Based on RFID Antenna for Detecting Mechanical Deformation," *IEEE Open Journal of Antennas and Propagation*, vol. 1, pp. 426–434, 2020.

[15] M. A. S. Tajin, C. E. Amanatides *et al.*, "Passive UHF RFID-based Knitted Wearable Compression Sensor," *IEEE Internet of Things Journal*, pp. 1–1, 2021.

[16] W. Wang, W. Zeng *et al.*, "Wireless Temperature Monitoring With Shape Memory Alloy-Based Antenna," *IEEE Antennas and Wireless Propagation Letters*, vol. 20, no. 3, pp. 313–316, 2021.

[17] F. Alimenti, V. Palazzi *et al.*, "A Wireless MEMS Humidity Sensor Based on a Paper-Aluminium Bimorph Cantilever," in *2021 IEEE MTT-S International Microwave Symposium (IMS)*, 2021, pp. 823–826.

[18] R. Raju, G. E. Bridges, and S. Bhadra, "Wireless passive sensors for food quality monitoring: Improving the safety of food products," *IEEE Antennas and Propagation Magazine*, vol. 62, no. 5, pp. 76–89, 2020.

[19] E. M. Amin, J. K. Saha, and N. C. Karmakar, "Smart Sensing Materials for Low-Cost Chipless RFID Sensor," *IEEE J. Sensors*, vol. 14 no. 7, pp. 2198 – 2207, 2014.

[20] R. Ramzan, M. Omar *et al.*, "Internet of Trees (IoTr) Implemented by Highly Dispersive Electromagnetic Sensors," *IEEE Sensors Journal*, vol. 21, no. 1, pp. 642–650, 2021.

[21] H. El Matbouly, S. Tedjini *et al.*, "Chipless sensing system compliant with the standard radio frequency regulations," *IEEE Journal of Radio Frequency Identification*, vol. 3, no. 2, pp. 83–90, 2019.

[22] C. Occhiuzzi and G. Marrocco, "Constrained-Design of Passive UHF RFID Sensor Antennas," *IEEE Transactions on Antennas and Propagation*, vol. 61, no. 6, pp. 2972–2980, 2013.

[23] J. Barreto, G. Perez *et al.*, "A study of wearable wireless power transfer systems on the human body," *IEEE Open Journal of Antennas and Propagation*, vol. 2, pp. 86–94, 2021.

[24] U. Hasni, M. E. Piper *et al.*, "Screen-printed fabric antennas for wearable applications," *IEEE Open Journal of Antennas and Propagation*, vol. 2, pp. 591–598, 2021.

[25] M. Wagih, A. S. Weddell, and S. Beeby, "Meshed High-Impedance Matching Network-Free Rectenna Optimized for Additive Manufacturing," *IEEE Open Journal of Antennas and Propagation*, vol. 1, pp. 615 – 626, 2020.

[26] B. Wiltshire, K. Mirshahidi *et al.*, "Robust and sensitive frost and ice detection via planar microwave resonator sensor," *Sensors and Actuators B: Chemical*, vol. 301, p. 126881, 2019.

[27] R. U. Tariq, M. Ye *et al.*, "Microwave sensor for detection of ice accretion on base station antenna radome," *IEEE Sensors Journal*, pp. 1–1, 2021.

[28] K. Zannas, H. El Matbouly *et al.*, "Self-Tuning RFID Tag: A New Approach for Temperature Sensing," *IEEE Transactions on Microwave Theory and Techniques*, vol. 66, no. 12, pp. 5885–5893, 2018.

[29] G. M. Bianco, S. Amendola, and G. Marrocco, "Near-Field Constrained Design for Self-Tuning UHF-RFID Antennas," *IEEE Transactions on Antennas and Propagation*, vol. 68, no. 10, pp. 6906–6911, 2020.

[30] J. Bonior, Z. Hu *et al.*, "Software-Defined-Radio-Based Wireless Tomography: Experimental Demonstration and Verification," *IEEE Geoscience and Remote Sensing Letters*, vol. 12, no. 1, pp. 175–179, 2015.

[31] S. Tedjini, N. Karmakar *et al.*, "Hold the Chips: Chipless Technology, an Alternative Technique for RFID," *IEEE Microwave Magazine*, vol. 14, no. 5, pp. 56–65, 2013.

[32] M. Wagih, A. S. Weddell, and S. Beeby, "Rectennas for RF Energy Harvesting and Wireless Power Transfer: a Review of Antenna Design [Antenna Applications Corner]," *IEEE Antennas Propag. Mag.*, vol. 62 no. 5, pp. 95 – 107, 2020.

[33] B.-C. Tseng, L.-C. Liao *et al.*, "Analytical solutions for the radiated emission of parallel microstrip traces," *IEEE Transactions on Electromagnetic Compatibility*, vol. 53, no. 3, pp. 842–845, 2011.

[34] E. Perret, S. Tedjini, and R. S. Nair, "Design of Antennas for UHF RFID Tags," *Proceedings of the IEEE*, vol. 100, no. 7, pp. 2330–2340, 2012.

[35] G. Marrocco, "Pervasive electromagnetics: sensing paradigms by passive RFID technology," *IEEE Wireless Communications*, vol. 17, no. 6, pp. 10–17, 2010.

[36] V. Palazzi, F. Alimenti *et al.*, "Zero-power, long-range, ultra low-cost harmonic wireless sensors for massively distributed monitoring of cracked walls," in *2017 IEEE MTT-S International Microwave Symposium (IMS)*, 2017, pp. 1335–1338.

[37] V. Komarov, S. Wang, and J. Tang, *Permittivity and Measurements*. American Cancer Society, 2005.

[38] R. Kozak, M. C. Jain *et al.*, "Durable Ice Sensors utilizing Microwave SRRs Coated with Protective Epoxy for De-Icing Control," in *2021 IEEE Sensors*, 2021, pp. 1–4.

[39] A. D. Boursianis, M. S. Papadopoulou *et al.*, "Multiband patch antenna design using nature-inspired optimization method," *IEEE Open Journal of Antennas and Propagation*, vol. 2, pp. 151–162, 2021.

[40] C. R. Paul, . Wiley, 2010.

[41] J. G. D. Hester and M. M. Tentzeris, "Inkjet-Printed Flexible mm-Wave Van-Atta Reflectarrays: A Solution for Ultralong-Range Dense Multitag and Multisensing Chipless RFID Implementations for IoT Smart Skins," *IEEE Trans. Microw. Theory Techn.*, vol. 64, 12, pp. 4763 – 4773, 2016.

[42] DuPont, "DuPont Kapton HN," 2019, Online: https://www.dupont.com/content/dam/dupont/amer/us/en/products/ei-transformation/documents/DEC-Kapton-HN-datasheet.pdf.

[43] M. Wagih, "Direct-Write Dispenser Printing for Rapid Antenna Prototyping on Thin Flexible Substrates," in *2020 European Conference on Antennas and Propagation (EuCAP)*, 2020.

[44] "Frozen pipes cause billions in damage, but can be prevented," *Insurance Journal*, 2006, Online: https://www.insurancejournal.com/magazines/mag-features/2006/01/02/64842.htm. [accessed: 12/03/2021.

[45] Y. Boussad, M. N. Mahfoudi *et al.*, "Evaluating smartphone accuracy for rssi measurements," *IEEE Transactions on Instrumentation and Measurement*, vol. 70, pp. 1–12, 2021.

[46] B. Biernacki, S. Zhang, and W. Whittow, "3d printed substrates with graded dielectric properties and their application to patch antennas," in *2016 Loughborough Antennas Propagation Conference (LAPC)*, 2016, pp. 1–5.

[47] P. Blasco, J. Palacios, and S. Schmitz, "Effect of icing roughness on wind turbine power production," *Wind Energy*, vol. 20, no. 4, pp. 601–617, 2017.

[48] L. Russell, R. Goubran *et al.*, "Agile IoT for Critical Infrastructure Resilience: Cross-Modal Sensing As Part of a Situational Awareness Approach," *IEEE Internet of Things Journal*, vol. 5, no. 6, pp. 4454–4465, 2018.

[49] X. Chen, A. Alghaihab *et al.*, "A Crystal-Less BLE Transmitter With Clock Recovery From GFSK-Modulated BLE Packets," *IEEE Journal of Solid-State Circuits*, vol. 56, no. 7, pp. 1963–1974, 2021.

[50] M. Wagih, Y. Wei *et al.*, "Reliable UHF Long-Range Textile-Integrated RFID Tag Based on a Compact Flexible Antenna Filament," *Sensors*, vol. 20 (12), p. 3435, 2020.

Mahmoud Wagih (GS'18, M'21) received his B.Eng. (Hons.) in September 2018, and his Ph.D. on rectenna design in April 2021, both in Electrical and Electronic Engineering from the University of Southampton.

In 2017 he worked as a Research Assistant at the University of Southampton Malaysia. In 2018, he was a Hardware Engineering Intern at Arm, and, in 2020, a Research Intern at Arm, Cambridge, U.K. He was a post-doctoral research fellow, in 2021, and a Senior Research Fellow, in 2022, at the University of Southampton, U.K. He is a currently a UK IC Research Fellow and Assistant Professor (Proleptic Lecturer) with the James Watt School of Engineering at the University of Glasgow. His interests broadly cover antennas and microwave systems for energy harvesting, sensing, and wearable applications. He has over 55 refereed journal and conference publications, and has delivered several invited talks on these topics.

Dr. Wagih was the recipient of the Best Undergraduate Project Prize, School Winner Doctoral Research Award, Best in Faculty Doctoral Research Award, and the Dean's Award for Early Career Researchers, in 2018-2021, at the University of Southampton. He received the Best Student Paper Award at the IEEE Wireless Power Transfer Conference, 2019, the Best Oral Presentation at PowerMEMS, 2019, the Best Paper Award at PowerMEMS, 2021, was a Best Student Paper Finalist at IEEE WPTC, 2021, received the IEEE MTT-S Best 3MT Presentation Prize (second place) at the IEEE Microwave Week, 2020, was a U.K. TechWorks Young Engineer of the Year finalist, in 2021, and received the EurAAP Per-Simon Kildal Award for the Best PhD in Antennas and Propagation, and a URSI Young Scientist Award, in 2022. He has serves as a TPC reviewer for various conferences including the IEEE International Microwave Symposium (IMS), and the IEEE Antennas and Propagation Symposium (APS) and a regular reviewer for 17 journals and Transactions. He is a Senior Member of the International Union of Radio Science (URSI) and a member of the Institute of Engineering and Technology (MIET). He is an affiliate member of the IEEE Microwave Theory & Techniques Technical Committees TC-25 and TC-26. He
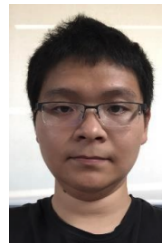
Junjie Shi received a B.Sc. degree from the Nanjing Institute of Technology, China in 2008, an M.Sc. degree in Microelectromechanical systems in 2012, and a Ph.D. in 2017 at the University of Southampton.

He was appointed as a Research Fellow in the School of Electronics and Computer Science (ECS) in 2017. His research interests covers a board range of wearables including but not limited to sensors, actuators, memory, and energy harvesting etc. As well as those wearable devices, he is interested in the fabrication technologies, such as 3D printing, dispenser printing, inkjet printing, micro-fabrications, which enable conventional and novel devices to be fabricated on textiles.